Journal of Theoretical Biology 558 (2023) 111356

Contents lists available at ScienceDirect

Journal of Theoretical Biology

journal homepage: www.elsevier.com/locate/yjtbi

Transplantation of fragments from different planaria: A bioelectrical model for head regeneration

Javier Cervera [a,*], José A. Manzanares [a], Michael Levin [b,c], Salvador Mafe [a]

[a] Dept. Termodinàmica, Facultat de Física, Universitat de València, E-46100 Burjassot, Spain
[b] Dept. of Biology and Allen Discovery Center at Tufts University, Medford, MA 02155-4243, USA
[c] Wyss Institute for Biologically Inspired Engineering, Harvard University, Boston, USA

ARTICLE INFO

Keywords:
Cell membrane potential
Multicellular polarity
Bioelectrical patterns
Planaria
Axial patterning
Implants and chimeras

ABSTRACT

Head-tail planaria morphologies are influenced by the electric potential differences across the animal's primary axis, as evidenced e.g. by voltage-sensitive dyes and functional experiments that create permanent lines of 2-headed but genetically wild-type animals. However, bioelectrical and biochemical models that make predictions on what would happen in the case of spatial chimeras made by tissue transplantation from different planaria (different species and head shapes) are lacking. Here, we use a bioelectrical model to qualitatively describe the effects of tissue transplantation on the shape of the regenerated head. To this end, we assume that the cells may have distinct sets of ion channels and ascribe the system outcome to the axial distributions of average cell potentials over morphologically relevant regions. Our rationale is that the distributions of signaling ions and molecules are spatially coupled with multicellular electric potentials. Thus, long-time downstream transcriptional events should be triggered by short-time bioelectrical processes. We show that relatively small differences between the ion channel characteristics of the cells could eventually give noticeable changes in the electric potential profiles and the expected morphological deviations, which suggests that small but timely bioelectrical actions may have significant morphological effects. Our approach is based on the observed relationships between bioelectrical regionalization and biochemical gradients in body-plan studies. Such models are relevant to regenerative, developmental, and cancer biology in which cells with distinct properties and morphogenetic target states confront each other in the same tissue.

1. Introduction

When planarian flatworms are cut into fragments, the resulting pieces can make a complete worm following morphological mechanisms still under discussion (Cebrià et al., 2018, Pezzulo and Levin, 2016). In particular, the number, location, and shape of heads have been experimentally and theoretically studied (Bischof et al., 2020, Cervera et al., 2020a, Cervera et al. 2021a, Durant et al., 2019, Emmons-Bell et al., 2015, Owlarn and Bartscherer, 2016, Pietak and Levin., 2018, Pietak et al., 2019, Saló et al., 2009). Distinct head–tail, no-head, and double-head axial morphologies are observed by controlling the electric potential differences across the animal's primary (anterior-posterior) axis as evidenced by voltage-sensitive dyes (Durant et al., 2017, Durant et al., 2019). The functional importance of this bioelectrical prepattern (Beane et al., 2011, Durant et al., 2017, Durant et al., 2019, Nogi and Levin, 2005, Pezzulo et al., 2021) was shown in experiments in which the number of heads in regenerating fragments was modulated by specifically altering ion channel function or gap junctional connectivity. In addition to the number of heads (and the patterning of the primary axis), different morphologies of planarian heads, the shapes of their brain, and distributions of stem cells are obtained after gap junction (GJ) blocking caused by octanol (Cervera et al., 2021, Emmons-Bell et al., 2015). In this case, the heads of wild-type, genomically-normal planaria can be remodeled to resemble those of different planaria species by temporarily disturbing the intercellular connectivity during regeneration (Emmons-Bell et al., 2015).

It has been proposed that bioelectric gradients, acting far earlier than the known (downstream) gene expression and morphogen distribution changes, are drivers of morphogenetic cues that enable fragments to rebuild a correct worm (Durant et al., 2017, Durant et al., 2019, Emmons-Bell et al., 2015). Also, the induced 2-head state is permanent -fragments of such worms continue to generate 2-headed worms in

* Corresponding author.
E-mail address: jcervera@uv.es (J. Cervera).

https://doi.org/10.1016/j.jtbi.2022.111356
Received 7 July 2022; Received in revised form 16 October 2022; Accepted 11 November 2022
Available online 17 November 2022

perpetuity, without any further manipulation (Durant et al., 2017, Oviedo et al., 2010). In contrast to other species (mouse, fruit fly, etc.) in which genetic lines of aberrant anatomy are readily obtained and kept, the 2-headed worms remain the only known stable line with abnormal anatomy in planaria. A key aspect of understanding the target morphologies reliably produced by independent cell activities is the delineation of collective decision-making that leads to specific shapes within a given context. Such information is best obtained by perturbing the system in ways that explore its behavior outside the one standard scenario of wild-type regeneration. A useful strategy in biology has been that of chimerism (Nanos and Levin, 2022) because by confronting cells and tissues with novel neighbors, insight can be gained into the ways in which growth and form depend on the properties of the cells. Although much information about the molecular steps guiding stem cell differentiation in planaria exist (Aboobaker, 2011, Hwang et al., 2015, Reddien et al., 2005), models that make predictions about what shapes will arise in chimeric scenarios are lacking.

Bioelectrical networks can provide useful qualitative ideas concerning the system morphology under different environmental constraints (Cervera et al., 2020b). We consider here model simulations that address what will happen if you mix cells from different planaria (different species and head shapes), e.g., what kind of head shape will result (Levin et al., 2019). In this way, we aim at qualitatively describing the effects of tissue transplantation on the shape of the regenerated head.

We employ a purely bioelectrical perspective (Fig. 1) as a complementary view to the biochemical (Cebrià et al., 2018, Stückemann et al., 2017) and biomechanical (Bischof et al., 2020, Leronni et al., 2020) descriptions. To this end, we focus on the cell bioelectrical characteristics of two species of decapitated flatworms with distinct head shapes (Fig. 1), assuming that the two cell types have different gene expressions which are specific to their respective morphologies (Levin et al., 2019). Thus, the cells may have different sets of ion channels and gap junctions (GJ) (Cervera et al., 2020b, Levin, 2021, Nogi and Levin, 2005).

While we incorporate in the model the cellular ion channel *hardware*, we analyze which shape would result from the heterogeneous mixture of Fig. 1 by focusing on the bioelectrical *software*, implemented here by the multicellular electrical signals that control the large-scale outcomes. In this way, we ascribe the morphological system outcome after transplantation to the axial distribution of cell potentials (Cervera et al., 2020a, Durant et al., 2017, Durant et al., 2019). The steady-state electrical potential profiles are obtained for the two decapitated planarians 1 and 2 from different species and compared with that of a chimera in which planarian 2′s cells are transplanted onto decapitated planaria 1. The deviation of the bioelectrical profile of the transplanted chimera planaria with respect to the decapitated planaria 1 is used to predict the transplanted planaria outcome (Fig. 1) because it is experimentally known that the distributions of signaling ions and molecules are spatially coupled with multicellular electric potentials (Cervera et al., 2020b, Durant et al., 2017, Levin, 2021). In this way, multicellular electric potentials can contribute to the distributed positional information (Cervera et al., 2019, Levin 2021) needed for development and regeneration.

Assuming that head regeneration occurs after transplantation, we predict the final head shape of the transplanted planaria on the basis of deviation criteria for the different steady-state potential distributions before and after the transplantation of Fig. 1. Certainly, this constitutes a simplifying model assumption. Note however that a large number of mechanisms relating bioelectrical cell states to biochemical downstream processes have been described; specifically, it has been shown in experiments *in vivo* that the bioelectric state regulates (and can even reverse) the downstream implementation machinery which includes biochemical, transcriptional, and likely biomechanical pathways (Cervera et al., 2020b, Durant et al., 2017, Durant et al., 2019, Emmons-Bell et al., 2015, Harris, 2021; Levin et al., 2019, Levin, 2021, Pai et al., 2020, Pezzulo et al., 2021, Pietak and Levin, 2018).

Our rationale here is that: (*i*) multicellular electrical potentials are morphologically instructive (Cervera et al., 2020b, Durant et al., 2017, Durant et al., 2019, Harris, 2021, Levin et al., 2019) and (*ii*) the short-term bioelectrical information eventually modulates the long-term transcriptional responses because of the coupling between the electric potential and the signaling ions (e.g., calcium) and molecules (e.g., serotonin) spatiotemporal distributions (Cervera et al., 2020b, Levin, 2021), as shown in Fig. 2. Thus, while the head morphology is not exclusively dependent on just the electric potential, the experimental fact is that cell potentials significantly influence crucial downstream biochemical and genetic responses in planaria. Note however that, in this model, we will put emphasis on the dynamics of bioelectrical patterns rather than on the biochemical processes that they can control downstream.

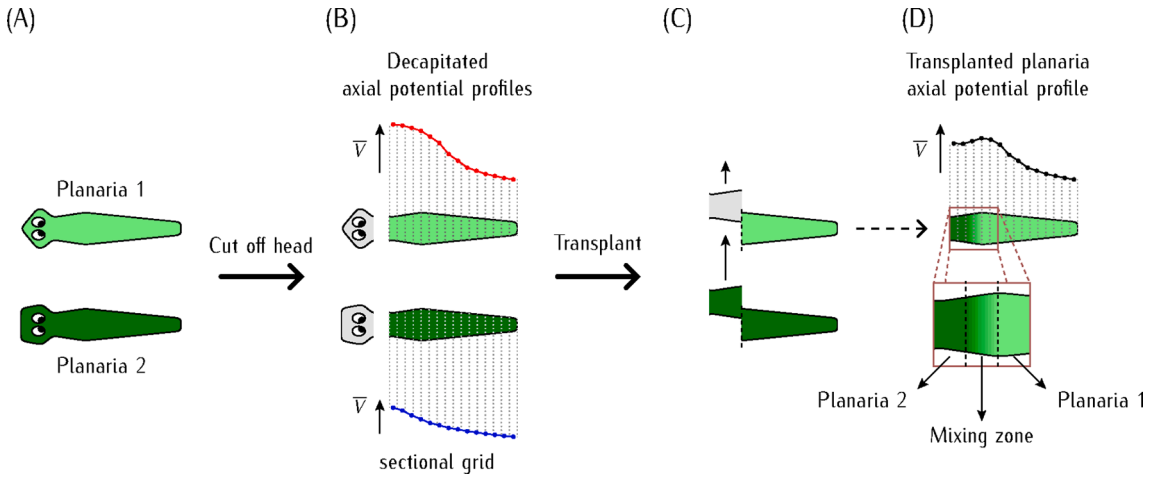

Fig. 1. (A) Schematic of the thought experiment involving two different planarian species with distinct head morphologies and similar tails. (B) The head region removed is assumed to amount to 20 % of the total multicellular aggregate. In the simulations, the different axial potential profiles obtained are supposed to be instructive for the distinct head anatomies. These axial potentials $\overline{V}$ are calculated by averaging the two-dimensional multicellular distribution at each point along the sectional grid. (C) After the two heads bisection, a percentage of the planaria 2 cells is transplanted into the removed trunk of the planaria 1. (D) The mixing zone in the transplanted planaria where limited cell mixing may occur. Because of the mechanical junctions between cells, the inter-diffusion of cells 1 and 2 should be limited to a relatively small mixing zone. We tentatively assume that this zone amounts to 10 % of the non-decapitated multicellular aggregate, which is significant but smaller than the two individual planaria fragments.

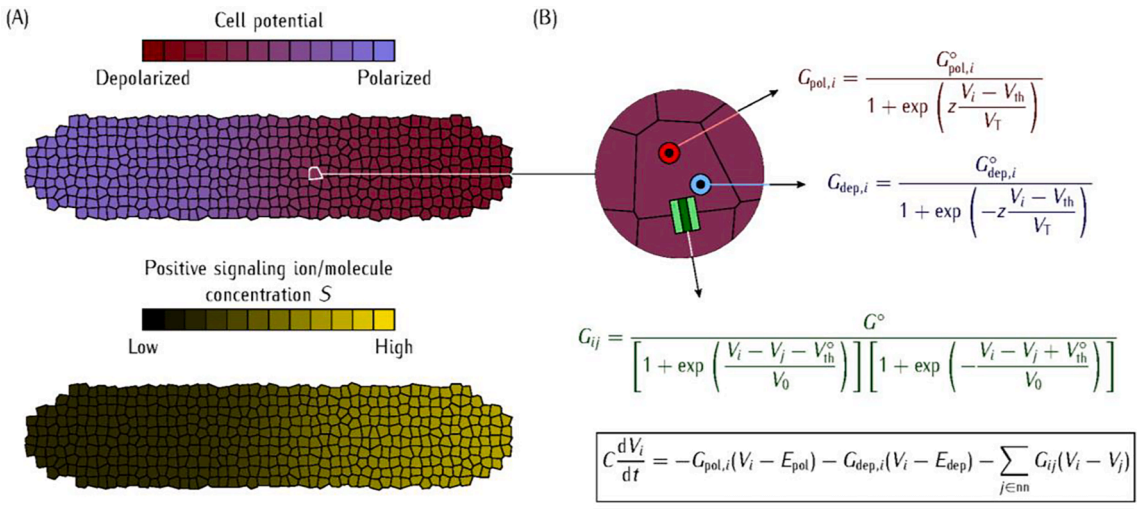

Fig. 2. (A) Schematic of the multicellular aggregate of $N = 500$ cell potentials. The cells are fixed in place with a fixed number of intercellular gap junctions. The concentration distribution S of a positively charged ion or molecule regulated by the electric potential is also shown for comparison. Particular examples of these signaling biochemical species can be found elsewhere (Aslanidi et al., 2001, Cervera et al., 2020b, Durant et al., 2017, Harris, 2021, Levin, 2021). (B) The ionic currents $I_{dep,i}$ and $I_{pol,i}$ flow through two generic depolarizing (*dep*) and polarizing (*pol*) voltage-gated channels when the cell potential V_i deviates from the respective equilibrium potentials E_{dep} and E_{pol}. Here, $G^{\circ}_{k,i}$ ($k = dep, pol$) is the maximum channel conductance, z is the gating charge number, V_{th} is the threshold potential, and $V_{\mathrm{T}} = RT/F$ is the thermal potential, where R is the gas constant, T is the temperature, and F is the Faraday constant (Cervera et al., 2020b). The intercellular current $G_{ij}(V_i - V_j)$ flows from cell i to its neighboring cell j through a gap junction with conductance $G_{ij} \leqslant G^{\circ}$, where G° is the maximum junction conductance. The potentials V_0 and V°_{th} characterize the junction conductance shape (Cervera et al., 2020b). This intercellular current flows between the central cell i and the $n \approx 4$ nearest-neighbor (nn) cells j. Note that each cell type 1 and 2 may have different channels and junction conductances.

2. Biophysical model

The complexity of the feedback between the spatial and time scales of transcriptional, mechanical, and electrical processes (Bischof et al., 2020, Capek and Müller, 2019, Herath and Lobo, 2020, Ivankovic et al., 2019, Owlarn and Bartscherer, 2016, Reddien, 2018, Stückemann et al., 2017, Williamson et al., 2021) makes a complete biological description difficult. Here, we concentrate on the electrical polarity only, establishing a minimal bioelectric framework sufficient to analyze the chimeric scenario, and assume that the different head morphologies arise from the bioelectrical signals and the resulting downstream biochemical processes. In this *short-term* approach, the number of model cells after transplantation is fixed and the subsequent *long-time* transcriptional and regeneration processes are ignored (Cervera et al., 2020b).

In this phenomenological model, the experimental outcomes of Fig. 1 depend on the relative contributions of the individual ion channel conductances and the intercellular gap junction conductance, as shown in Fig. 2 (Cervera et al., 2020a). From an instructive bioelectrical perspective (Cervera et al. 2020b, Levin, 2021), the multicellular electric patterns control the system morphology through the interplay between the individual cell ion channels that establish the electric potential difference across the membrane and the intercellular gap junctions that propagate the single-cell states to their neighbors (Durant et al., 2017, Durant et al., 2019, Emmons-Bell et al., 2015).

Fig. 2 shows a multicellular aggregate characterized by the single-cell potentials $V_i < 0$, $i = 1, 2, \ldots, N$ (Cervera et al., 2020a). The electric potential pattern can be visualized by using voltage-sensitive dyes (Durant et al. 2019, Lazzari-Dean et al., 2021, Levin, 2021). The cell potentials depend on the dynamic current balance modulated by two generic depolarizing and polarizing channels together with the intercellular currents through the gap junctions established between neighboring cells (Cervera et al., 2020b). Analogously, counteracting voltage-gated channels and synaptic junctions modulate the cell excitability and plasticity of neural networks, respectively.

In a real cell, there is a myriad of membrane channels and ion transporters. The polarizing (*pol*) voltage-gated channel in Fig. 2 represents the whole class of (hyper-)polarizing channels that act to establish an effective equilibrium potential E_{pol}. Similarly, the depolarizing (*dep*) channel in Fig. 2 represents the whole class of depolarizing channels that act to establish an effective equilibrium potential E_{dep}. These potentials, which characterize the polarized and depolarized cell bioelectrical states depend on the external and cell inside ionic concentrations that are assumed to be constant here. The model cell capacitance C parametrizes the cell sensitivity to bioelectrical signals. The simulation conditions are briefly described in the *Methods* section.

3. Results and discussion

Fig. 3 shows the cell potential distributions for planarias 1 and 2 before transplantation together with those obtained for the transplanted planaria after insertion (Fig. 1). Note the different axial distributions assumed for the *dep* channel conductance of planarias 1 and 2 in Fig. 3. Because the two cell types should have different gene expressions which are specific to the respective planaria morphologies (Levin et al., 2019), it is reasonable to assume that these cells may show distinct sets of ion channels (Cervera et al., 2020b, Levin, 2021). We may consider that the differences between the cells channel characteristics could be either qualitative (i.e., different genes and protein ion channels) or quantitative (i.e., genes with different expression levels). Experimentally, the interplay between two voltage-gated depolarizing channels (Wheeler et al., 2012) with different axial localizations (Zhang et al., 2011) has been found to influence planarian polarity because of the calcium-controlled local gene expression.

We need now to define deviation criteria to extract morphological consequences from the simulations. In biochemical models, instructive information can be obtained from the concentration profiles of signaling molecules over morphologically significant regions (Cervera et al., 2021, Herath and Lobo, 2020, Werner et al., 2015). Analogously, we assume here that the electric potential over the left fragment of the transplanted system is crucial to the subsequent head development. Thus, Fig. 4 shows the axial potential profiles, together with the results of averaging these potentials over this fragment, for different transplantation percentages parametrized by the relative size of the

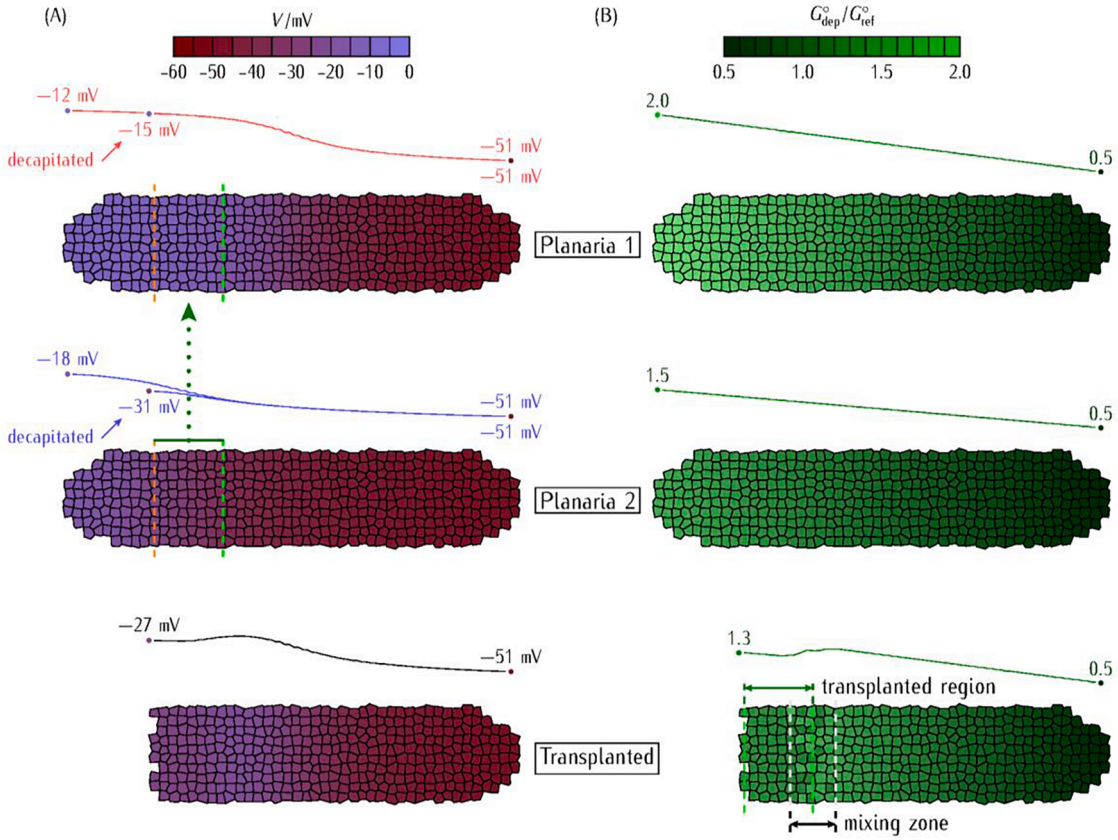

Fig. 3. (A) The electric potentials V_i of the cells of planarias 1 and 2, both before and after decapitation, together with the resulting steady-state values obtained for the transplanted planaria. (B) The corresponding *dep* channel conductance distributions that give rise to the cell potentials. The lines above the multicellular aggregate show the axial profiles of these bioelectrical magnitudes. Note that the single-cell characteristics $z = 2$ and $V_{th} = -V_T = -RT/F = -27$ mV are the same for both channels. For the *pol* channel, we use $E_{pol} = -55$ mV and $G^{\circ}_{pol}/G^{\circ}_{ref} = 1$, where G°_{ref} is a reference conductance. For the *dep* channel, however, we use $E_{dep} = -5$ mV and consider the different $G^{\circ}_{dep}/G^{\circ}_{ref}$ axial profiles shown in the figure to characterize the distinct planarias 1 and 2. For the gap junction conductance of Fig. 2, we assume also the common values $G^{\circ}/G^{\circ}_{ref} = 1$, $V_0 = 10$ mV, and $V^{\circ}_{th} = 20$ mV.

transplanted trunk. The numbers in the 4 × 4 panels of Fig. 4 quantify the deviation between the transplanted planaria and the decapitated planaria 1. Note that the deviation index could be interpreted not only as the most probable head outcome but also as a measure of intermediate morphological outcomes.

The experimental variability associated with cutting and transplantation makes it necessary to introduce some stochastic characteristics in the mixing zone. On the opposite side, however, the zone characteristics should be approximately specified to allow a direct comparison between simulations. Taking advantage of the two-dimensional geometry of the mixing zone (Figs. 2 and 3), we consider different distributions for the cell concentration in the cross-section but force them to follow a linear probability distribution along the mixing zone axis in the simulations. This stochastic characteristic of the model is clearly shown by the different results obtained in Fig. 4 for the case of four distinct mixing zones at fixed transplantation percentage. As expected, the relative axial potential differences obtained tend to decrease with the transplanted percentage because of the concomitant increase in the absolute number of planaria 2 cells contributing to this potential.

The results of Fig. 4 are summarized in Fig. 5, which provides estimations of the expected deviations between the transplanted planaria and the planaria 1 heads for different transplanted percentages of planaria 2 and three degrees of intercellular connectivity. These deviations are estimated from the deviation index of Fig. 4, which is based on the different axial potentials averaged over the left region of the system. As expected, the deviations increase with the transplanted percentage and decrease with the multicellular aggregate connectivity because of the bioelectrical buffer effect due to planaria 1 counteracting the inserted planaria 2 perturbation.

Note the wide range of intermediate values obtained for the percentage deviations in the expected transplanted planaria head (Fig. 5). While the model may ascribe these values to the probabilities of obtaining the planaria 2 morphology after transplantation, there is also a possibility of intermediate morphologies. Note also that the network effects derived from changes in the gap junction conductance can significantly influence the biosystem dynamics and the morphology outcomes (Cervera et al., 2020c, Cervera et al., 2021, Emmons-Bell et al., 2015, Riol et al., 2021). In particular, the connectivity provided by the intercellular junctions can also influence the planaria head morphology, as shown experimentally (Emmons-Bell et al., 2015) and theoretically (Cervera et al., 2021) in junction blocking studies.

4. Conclusions

Head-tail planaria morphologies are influenced by the electric potential difference between the axial extremes, as evidenced by voltage-sensitive dyes (Durant et al., 2017, Durant et al., 2019) and originally identified by applied field effects (Lange and Steele, 1978, Marsh and Beams, 1952). We have employed a biophysical approach to qualitatively describe the effects of fragment transplantation on head regeneration when different cell types of planaria are present (Fig. 1). As a complementary view to the dominant biochemical descriptions (Adell et al., 2010, Meinhardt, 2008), we concentrate on the bioelectrical characteristics by assuming that the different cells may have distinct sets of ion channels. We ascribe the system outcome to the axial distributions of average cell potentials over morphologically relevant regions. Our

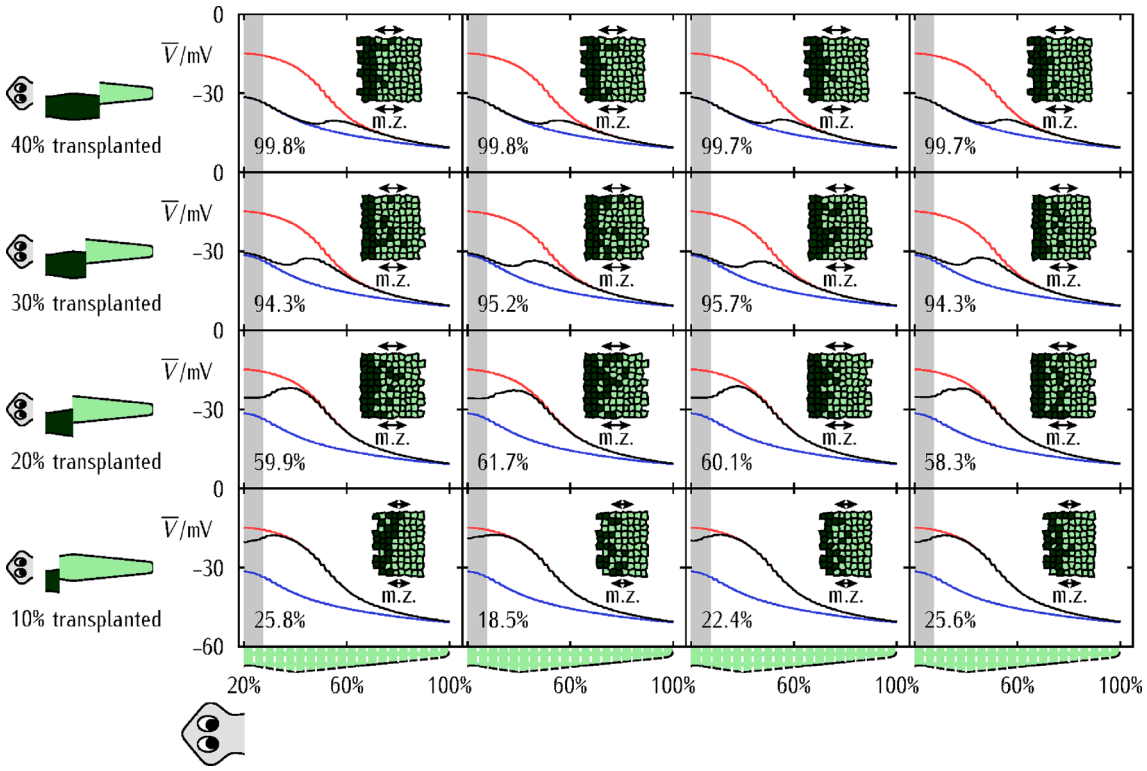

Fig. 4. The axial potential $\overline{V}$ (*black curves*) of the transplanted planaria *vs* position for different sizes of the transplanted trunk of planaria 2 (*rows,* 10–40 % percentages) and different compositions of the mixing zone (*columns*). The curves describing the axial potential $\overline{V}$ of the decapitated planarias 1 (*top*, *red*) and 2 (*bottom*, *blue*) are the same in all panels. The percentage shown in each panel is the *deviation index* $100\,\%|\langle\overline{V_t}\rangle - \langle\overline{V_1}\rangle|/|\langle\overline{V_2}\rangle - \langle\overline{V_1}\rangle|$, where $\langle\overline{V_t}\rangle$, $\langle\overline{V_1}\rangle$, and $\langle\overline{V_2}\rangle$ are average values of $\overline{V}$ over the 10 % left region (*shadowed*) of the transplanted, decapitated 1, and decapitated 2 planarias, respectively. This index serves as a predictive system outcome, because a large value of the index indicates that the transplanted planaria deviates significantly from decapitated planaria 1 and resembles decapitated planaria 2. The *mixing zone* (m. z.) contains cells from the receiver (planaria 1, *light green*) and the donor (planaria 2, *dark green*) planaria, as shown in the insets. The cell composition in the m. z. is generated randomly (see *Methods*). The m. z. is centered at the right end of the transplanted region and its size is 10 % of the planaria length. The system parameters used are those of Fig. 2.

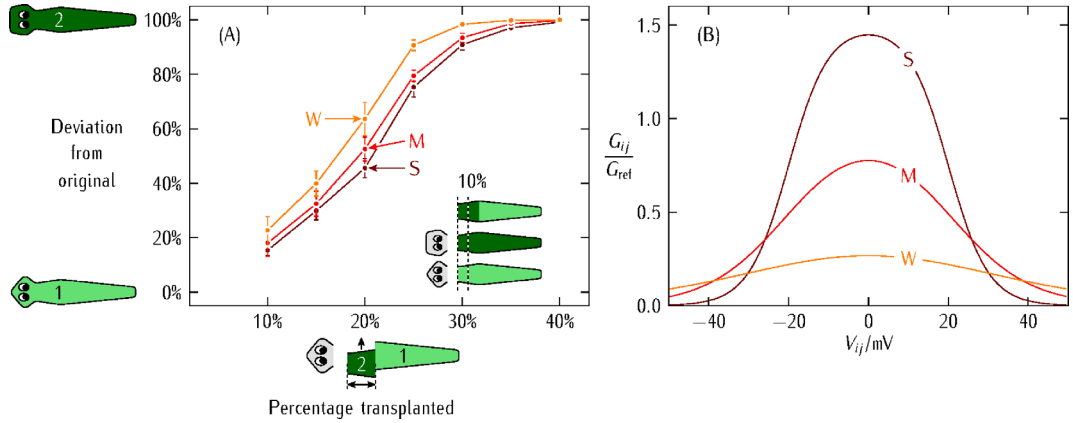

Fig. 5. (A) Estimated percentage deviation of the expected transplanted planaria head with respect to that of the planaria 1 as a function of the planaria 2 transplanted percentage. The curve is obtained from the deviation indexes of Fig. 4 and three distinct (weak, W; medium, M; strong, S) intercellular connectivities. The results correspond to 10 simulations with different mixing zones (Fig. 1) at each percentage transplanted. The central dot is the average value between the maximum and minimum values shown by the error bars. The inset shows the 10 % left fragment where the axial potentials are averaged. (B) The multicellular aggregate connectivities are parametrized by three voltage-gated conductances in the model of Fig. 2, where V_{ij} is the intercellular potential across the gap junction. The junction conductance parameters are $G^{\circ}/G^{\circ}_{\rm ref} = 0.5$ and $V_0 = 20$ mV (weak connectivity), $G^{\circ}/G^{\circ}_{\rm ref} = 1$ and $V_0 = 10$ mV (medium connectivity), and $G^{\circ}/G^{\circ}_{\rm ref} = 1.5$ and $V_0 = 5$ mV (strong connectivity). The channel conductances parameters are those of Figs. 2–4.

rationale here is that the instructive signaling ions and molecules distributions are spatially coupled with the multicellular electric potentials. Thus, long-time downstream transcriptional events should be triggered by short-time bioelectrical processes.

It may be surprising that a relatively small difference between the ion channel characteristics of cells # 1 and # 2 (Fig. 3) could eventually give noticeable changes in the electric potential profiles (Fig. 4) and the expected morphological deviations (Fig. 5). It is important to realize that

local bioelectrical perturbations are the initial step for the system outcome to be established downstream: the new electric potential pattern is instructive because it triggers subsequent biochemical processes that lead to the final morphology (Cervera et al., 2020b, Levin, 2021). For instance, it has been shown that even a single ion channel mRNA can induce very significant morphogenetic changes such as the induction of whole eyes in ectopic locations (Pai et al., 2012) or the repair of complex brain defects (Pai et al., 2020), which suggests that small but timely bioelectrical actions may have significant morphological effects. Note also that spatial correlations between neighboring cells are crucial for establishing patterns at both the local level and the overall system (Cervera et al., 2020b, Glen et al., 2018, Sajid et al., 2021). These experimental facts show the inherent capacity of multicellular systems to transit different configuration spaces (Fields and Levin, 2022) and clearly suggest that bioelectricity should contribute to the combination of plasticity and robustness characteristic of morphology (Cervera et al., 2020b, Levin, 2021).

The model simulations are not without limitations. For instance, we use only a small number of cells and have not considered the time-dependent regeneration process (Herath and Lobo, 2020, Werner et al., 2015), attempting to emphasize those bioelectrical parameters (Figs. 2 and 3) that can be manipulated to obtain the different morphologies (Figs. 4 and 5). Also, other relevant polarity effects concerning flow driven by the multiciliated epithelium and the nervous system role (Bischof et al., 2020) are ignored. Despite these limitations, this theoretical approach offers testable predictions concerning morphological outcomes and can be developed further, e.g. by considering distinct sets of gap junctions (Figs. 2 and 5) and by integrating together the initial bioelectrical regionalization with the subsequent long-time biochemical gradients in more complete body-plan studies. Most importantly, it provides a framework for understanding large-scale outcomes of morphogenesis in scenarios where tissues have distinct target morphologies. Subsequent experiments in planarian and other models will test these predictions, toward developing a better understanding of the control of emergent large-scale growth and form.

5. Methods

The simulation conditions are now briefly described. The ensemble of cells was constructed by generating a Voronoi diagram in 2D from a seed of points that form a square grid with a 25 % randomness over their position. The Voronoi diagram gives the different regions of cells including its vertices and edges. Two neighboring cells share one edge. The final ensemble is cut off from the Voronoi diagram. In every transplantation, the donor and receiver cell ensembles have the same geometry.

Once the geometry is determined, we give to every cell the particular bioelectrical parameters that correspond to its central position in the ensemble (Fig. 3). Initially (time $t = 0$), the steady-state potential of the single-cell isolated from its neighbors is used. In those cases where there are more than one steady-state potential (the bi-stable region; see Cervera et al. 2020a), the depolarized value is selected. Then the cells are "connected" to their neighbors and the systems are left to evolve for 100 times the characteristic bioelectric time. For typical values of $C = 10$ nF and $G^{\circ}_{\mathrm{ref}} = 1$ nS, the characteristic bioelectric time is $C/G^{\circ}_{\mathrm{ref}} = 10$ s. The evolution of the system is calculated from the equations of Fig. 2 using a finite-difference scheme. First, a maximum time variation for the cell potential is set at $V_{\max} = 10^{-3}$ mV together with a minimum and maximum time steps $\Delta t_{\min} = 10^{-3}\left(C/G^{\circ}_{\mathrm{ref}}\right)$ and $\Delta t_{\max} = 10^{2}\left(C/G^{\circ}_{\mathrm{ref}}\right)$, respectively. Then, for each simulation time, the time variation of every cell potential V_i is calculated from the equation of Fig. 2. The time step is obtained as $\Delta t = \min[\mathrm{d}V_i/\mathrm{d}t]/V_{\max}$ for all i, but keeping $\Delta t_{\min} \leqslant \Delta t \leqslant \Delta t_{\max}$. Then both the time and the cell potentials are updated as $t \rightarrow t + \Delta t$ and $V_i \rightarrow V_i + (\mathrm{d}V_i/\mathrm{d}t)\Delta t$ respectively. The calculation proceeds until the desired time is reached. Once the time is reached, we eliminate the cells of the head (the most-left 20 % of the ensemble) and left the system evolve for another 100 times the characteristic bioelectric time.

The transplantation starts by selecting the zone to be transplanted by indicating the position x_{cut} of the trunk cut off from the donor ensemble. Then, the transplanted zone is divided into two sections based on the average axial position x_{cell} of the cell. If $x_{\mathrm{cell}} < x_{\mathrm{cut}} - 0.05L$ (5 % of the ensemble), the cell of the donor ensemble replaces that of the receiver ensemble. If $x_{\mathrm{cut}} - 0.05L < x_{\mathrm{cell}} < x_{\mathrm{cut}} + 0.05L$ (mixing zone), we proceed to generate a random number r. Only if $r < (x_{\mathrm{cut}} + 0.05L - x_{\mathrm{cell}})/0.1L$, the cell is transplanted; otherwise, the original cell remains in its original place. Once the transplantation is completed, the ensemble 1 is left to evolve other 100 times the characteristic bioelectric time. Note that the use of random generated numbers makes every transplantation different.

The average potential profile of Figs. 3 and 4 is calculated by dividing the length of the decapitated ensemble into 100 different sections. Then, the average potential of every section $\overline{V}$ is calculated from the cells whose center is located within the section. The mean value $\langle \overline{V} \rangle$ used for the deviation index of Figs. 4 and 5 is obtained by averaging the potential of all the cells whose coordinate x_{cell} is within the initial 10 % of the decapitated ensemble.

CRediT authorship contribution statement

Javier Cervera: Methodology, Software, Formal analysis, Writing – review & editing. **José A. Manzanares:** Formal analysis, Writing – review & editing. **Michael Levin:** Conceptualization, Formal analysis, Writing – review & editing. **Salvador Mafe:** Conceptualization, Methodology, Formal analysis, Writing – original draft.

Declaration of Competing Interest

The authors declare that they have no known competing financial interests or personal relationships that could have appeared to influence the work reported in this paper.

Acknowledgments

J. C., J. A. M., and S. M. acknowledge the *Ministerio de Ciencia e Innovación* (Spain) and the European Regional Development Funds (FEDER), project No. PGC2018-097359-B-I00. M. L. acknowledges the support by the Templeton World Charity Foundation (TWCF0606) and the Guy Foundation Family Trust 103733-00001.

References

Aboobaker, A.A., 2011. Planarian stem cells: a simple paradigm for regeneration. Trends Cell Biol. 21, 304–311.
Adell, T., Cebrià, F., Saló, E., 2010. Gradients in planarian regeneration and homeostasis. Cold Spring Harb. Perspect. Biol. 2.
Aslanidi, O.V., Mornev, O.A., Skyggebjerg, O., Arkhammar, P., Thastrup, O., Sørensen, M.P., Christiansen, P.L., Conradsen, K., Scott, A.C., 2001. Excitation wave propagation as a possible mechanism for signal transmission in pancreatic Islets of Langerhans. Biophys. J. 80, 1195–1209.
Beane, W.S., Morokuma, J., Adams, D.S., Levin, M., 2011. A chemical genetics approach reveals H, K-ATPase-mediated membrane voltage is required for planarian head regeneration. Chem. Biol. 18, 77–89.
Bischof, J., Day, M.E., Miller, K.A., LaPalme, J., Levin, M., 2020. Nervous system and tissue polarity dynamically adapt to new morphologies in planaria. Dev. Biol. 467, 51–65.
Capek, D., Müller, P., 2019. Positional information and tissue scaling during development and regeneration. Development 146, dev177709. https://doi.org/10.1242/dev.177709.
Cebrià, F., Adell, T., Saló, E., 2018. Rebuilding a planarian: from early signaling to final shape. Int. J. Dev. Biol. 62, 537–550.
Cervera, J., Pai, V.P., Levin, M., Mafe, S., 2019. From non-excitable single-cell to multicellular bioelectrical states supported by ion channels and gap junction proteins: electrical potentials as distributed controllers. Progress Biophys. Mol. Biol. 49, 39–53.
Cervera, J., Meseguer, S., Levin, M., Mafe, S., 2020a. Bioelectrical model of head-tail patterning based on cell ion channels and intercellular gap junctions. Bioelectrochem. 132, 107410.

Cervera, J., Levin, M., Mafe, S., 2020b. Bioelectrical coupling of single-cell states in multicellular systems. J. Phys. Chem. Lett. 11, 3234–3241.
Cervera, J., Ramirez, P., Levin, M., Mafe, S., 2020c. Community effects allow bioelectrical reprogramming of cell membrane potentials in multicellular aggregates: Model simulations. Phys. Rev. E 102, 052412.
Cervera, J., Levin, M., Mafe, S., 2021. Morphology changes induced by intercellular gap junction blocking: A reaction-diffusion mechanism. Biosystems 209, 104511.
Durant, F., Morokuma, J., Fields, C., Williams, K., Adams, D.S., Levin, M., 2017. Long-term, stochastic editing of regenerative anatomy via targeting endogenous bioelectric gradients. Biophys. J. 112, 2231–2243.
Durant, F., Bischof, J., Fields, C., Morokuma, J., LaPalme, J., Hoi, A., Levin, M., 2019. The role of early bioelectric signals in the regeneration of planarian anterior/posterior polarity. Biophys. J. 116, 948–961.
Emmons-Bell, M., Durant, F., Hammelman, J., Bessonov, N., Volpert, V., Morokuma, J., Pinet, K., Adams, D.S., Pietak, A., Lobo, D., Levin, M., 2015. Gap junctional blockade stochastically induces different species-specific head anatomies in genetically wild-type Girardia dorotocephala flatworms. Int. J. Mol. Sci. 16, 27865–27896.
Fields, C., Levin, M., 2022. Competency in navigating arbitrary spaces as an invariant for analyzing cognition in diverse embodiments. Entropy 24, 819.
Glen, C.M., McDevitt, T.C., Kemp, M.L., 2018. Dynamic intercellular transport modulates the spatial patterning of differentiation during early neural commitment. Nat. Commun. 9, 4111.
Harris, M.P., 2021. Bioelectric signaling as a unique regulator of development and regeneration. Development 148, dev180794. https://doi.org/10.1242/dev.180794.
Herath, S., Lobo, D., 2020. Cross-inhibition of Turing patterns explains the self-organized regulatory mechanism of planarian fission. J. Theo. Biol. 485, 110042.
Hwang, B., An, Y., Agata, K., Umesono, Y., 2015. Two distinct roles of the yorkie/yap gene during homeostasis in the planarian Dugesia japonica. Dev. Growth Differ. 57, 209–217.
Ivankovic, M., Haneckova, R., Thommen, A., Grohme, M.A., Vila-Farré, M., Werner, S., Rink, J.C., 2019. Model systems for regeneration: planarians. Development 146, dev167684.
Lange, C.S., Steele, V.E., 1978. The mechanism of anterior-posterior polarity control in planarians. Differentiation 11, 1–12.
Lazzari-Dean, J.R., Gest, A.M.M., Miller, E.W., 2021. Measuring absolute membrane potential across space and time. Annu. Rev. Biophys. 50, 447–468.
Leronni, A., Bardella, L., Dorfmann, L., Pietak, A., Levin, M., 2020. On the coupling of mechanics with bioelectricity and its role in morphogenesis. J. R. Soc. Interface 17, 20200177.
Levin, M., 2021. Bioelectric signaling: Reprogrammable circuits underlying embryogenesis, regeneration, and cancer. Cell 184, 1971–1989.
Levin, M., Pietak, A., Bischof, J., 2019. Planarian regeneration as a model of anatomical homeostasis: Recent progress in biophysical and computational approaches. Semin. Cell Dev. Biol. 87, 125–144.
Marsh, G., Beams, H.W., 1952. Electrical control of morphogenesis in regenerating dugesia tigrina. I. Relation of axial polarity to field strength. J. Cell. Comp. Physiol. 39, 191–213.
Meinhardt, H., 2008. Models of biological pattern formation: from elementary steps to the organization of embryonic axes. Curr. Top. Dev. Biol. 81, 1–63.
Nanos, V., Levin, M., 2022. Multi-scale Chimerism: An experimental window on the algorithms of anatomical control. Cells Dev. 169, 203764.
Nogi, T., Levin, M., 2005. Characterization of innexin gene expression and functional roles of gap-junctional communication in planarian regeneration. Dev. Biol. 287, 314–335.
Oviedo, N., Morokuma, J., Walentek, P., Kema, I.P., Gu, M.B., Ahn, J.S., Hwang, J.S., Gojobori, T., Levin, M., 2010. Long-range neural and gap junction protein-mediated cues control polarity during planarian regeneration. Dev. Biol. 339, 188–199.
Owlarn, S., Bartscherer, M., 2016. Go ahead, grow a head! A planarian's guide to anterior regeneration. Regeneration (Oxf) 3, 139–155.
Pai, V.P., Cervera, J., Mafe, S., Willocq, V., Lederer, E.K., Levin, M., 2020. HCN2 channel-induced rescue of brain teratogenesis via local and long-range bioelectric repair. Front. Cell Neurosci. 14, 136.
Pai, V.P., Aw, S., Shomrat, T., Lemire, J.M., Levin, M., 2012. Transmembrane voltage potential controls embryonic eye patterning in Xenopus laevis, Development, 139 313-323, https://doi.org/10.1242/dev.073759. Erratum in: Development, 139 (2012) 623, https://doi.org/10.1242/dev.077917.
Pezzulo, G., LaPalme, J., Durant, F., Levin, M., 2021. Bistability of somatic pattern memories: stochastic outcomes in bioelectric circuits underlying regeneration. Philos. Trans. R. Soc. Lond. B Biol. Sci. 376, 0190765.
Pezzulo, G., Levin, M., 2016. Top-down models in biology: explanation and control of complex living systems above the molecular level. J. R. Soc. Interface 13 (124), 20160555.
Pietak, A., Levin, M., 2018. Bioelectrical control of positional information in development and regeneration: A review of conceptual and computational advances. Prog. Biophys. Mol. Biol. 137, 52–68.
Pietak, A., Bischof, J., LaPalme, J., Morokuma, J., Levin, M., Umulis, D., 2019. Neural control of body-plan axis in regenerating planaria. PLoS Comput. Biol. 15 (4), e1006904.
Reddien, P.W., 2018. The cellular and molecular basis for planarian regeneration. Cell 175, 327–345.
Reddien, P.W., Oviedo, N.J., Jennings, J.R., Jenkin, J.C., Sánchez Alvarado, A., 2005. SMEDWI-2 is a PIWI-like protein that regulates planarian stem cells. Science 310, 1327–1330.
Riol, A., Cervera, J., Levin, M., Mafe, S., 2021. Cell systems bioelectricity: how different intercellular gap junctions could regionalize a multicellular aggregate. Cancers (Basel) 13, 5300.
Sajid, N., Convertino, L., Friston, K., 2021. Cancer niches and their kikuchi free energy. Entropy 23, 609.
Saló, E., Abril, J.F., Adel, T., Cebrià, F., Eckelt, K., Fernandez-Taboada, E., Handberg-Thorsager, M., Iglesias, M., Molina, M.D., Rodríguez-Esteban, G., 2009. Planarian regeneration: achievements and future directions after 20 years of research. Int. J. Dev. Biol. 53, 1317–1327.
Stückemann, T., Cleland, J.P., Werner, S., Thi-Kim, V.H., Bayersdorf, R., Liu, S.Y., Friedrich, B., Jülicher, F., Rink, J.C., 2017. Antagonistic self-organizing patterning systems control maintenance and regeneration of the anteroposterior axis in planarians. Dev. Cell. 40, 248–263.
Werner, S., Stückemann, T., Beirán Amigo, M., Rink, J.C., Jülicher, F., Friedrich, B.M., 2015. Scaling and regeneration of self-organized patterns. Phys. Rev. Lett. 114, 138101.
Wheeler, D.G., Groth, R.D., Ma, H., Barrett, C.F., Owen, S.F., Safa, P., Tsien, R.W., 2012. CaV1 andCaV2 channels engage distinct modes of Ca2+ signaling to control CREB-dependent gene expression. Cell 149, 1112–1124.
Williamson, C., Chamberlin, H.M., Dawes, A.T., 2021. Coordination of local and long range signaling modulates developmental patterning. J. Theor. Biol. 517, 110596.
Zhang, D., Chan, J.D., Nogi, T., Marchant, J.S., 2011. Opposing roles of voltage-gated Ca^{2+} Channels in neuronal control of regenerative patterning. J. Neurosci. 31, 15983–15995.